Electronic, Crystal Chemistry, and Nonlinear Optical Property Relationships in the Dugganite $A_3B_3CD_2O_{14}$ Family

Hongwei Yu,[†] Joshua Young,[‡] Hongping Wu,[†] Weiguo Zhang,[†] James M. Rondinelli,*[,‡] and P. Shiv Halasyamani*[,†]

[†]Department of Chemistry, University of Houston, 112 Fleming Building, Houston, Texas 77204-5003, United States

[‡]Department of Materials Science and Engineering, Northwestern University, 2220 Campus Drive, Evanston, Illinois 60208-3108, United States

S Supporting Information

ABSTRACT: A family of six nonlinear optical (NLO) materials, $A_3B_3CD_2O_{14}$ (A = Sr, Ba, or Pb; B = Mg or Zn; C = Te or W; and D = P or V), has been synthesized and characterized. In addition to the synthesis and crystal structures, comprehensive characterization of these compounds includes second harmonic generation (SHG) measurements, theoretical calculations, infrared and diffuse reflectance spectroscopies, and thermogravimetric measurements. We find that all of the reported materials are SHG-active at 1064 nm, with responses ranging from 2.8 to 13.5 × KDP, and exhibit absorption edges in the mid- to deep-ultraviolet regime. By systematically replacing the A, B, C, and D cations, we are able to tune these properties and investigate the role of different NLO-active structural units in producing the SHG responses. Specifically, our electronic structure calculations reveal that the presence of Pb^{2+} on the A-site and Te^{6+} on the C-site is critical for generating a large SHG response. The synthesis and structure−property relationships described in this family of materials will enable the design and discovery of new NLO materials.
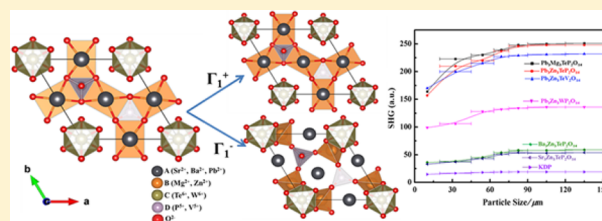
INTRODUCTION

Coherent light generated by solid-state lasers is widely used in a variety of fields ranging from medical therapies to materials processing as well as information communications.[1] However, the required wavelengths for these applications cannot always be directly generated from a convenient laser source, making the second harmonic generation (SHG) response of nonlinear optical (NLO) materials an essential alternative approach.[2] Over the years, a series of NLO crystals have been discovered, including β-BaB$_2$O$_4$ (BBO),[3a] LiB$_3$O$_5$ (LBO),[3b] CsLiB$_6$O$_{10}$ (CLBO),[3d] KBe$_2$B$_3$O$_6$F$_2$ (KBBF),[3e] KH$_2$PO$_4$ (KDP),[3f] and KTiOPO$_4$ (KTP).[3f] These materials, however, are unable to fully satisfy all demands imposed by the various desired application wavelengths and stability criteria under operation. As such, new high-performance NLO materials are of current academic and commercial interests.[4−12]

For NLO materials in the ultraviolet (UV) regime ($\lambda <$ 400 nm), borates are commonly used, such as Na$_3$Sr$_3$Be$_3$B$_3$O$_9$F$_4$,[4a] Na$_2$CsBe$_6$B$_5$O$_{15}$,[4b] K$_3$B$_6$O$_{10}$Cl,[5b] Ba$_4$B$_{10}$O$_{11}$F,[5c] Cs$_2$B$_4$SiO$_9$,[6b] and Li$_4$Sr(BO$_3$)$_2$.[6c] This is attributable to both their non-centrosymmetric (NCS) structure—a requirement for SHG—and their optical transparency and moderate birefringence (necessary for phase-matching). In addition, borates tend to be thermally stable and are amenable to growth of large single crystals.[3−6] Another materials class with UV NLO applications is the phosphates,[7] which generally exhibit SHG responses weaker than those of borates.[6−8] We recently combined anionic groups present in both of these families to produce Ba$_3$(ZnB$_5$O$_{10}$)PO$_4$

(BZBP), a new deep-UV NLO material with an absorption edge of 180 nm.[8]

SHG responses can be further enhanced by introducing other NLO-active structural units,[10−13] such as cations susceptible to second-order Jahn−Teller (SOJT) distortions, that is, octahedrally coordinated d^0 transition metals (Ti^{4+}, Nb^{5+}, W^{6+}, etc.),[10] or with a stereoactive lone pair (Pb^{2+}, Sn^{2+}, Se^{4+}, Te^{4+}, etc.).[11] In addition, Inaguma[12b] and Chen[3] also reported that the displacement of a d^{10} cation can support a large SHG response. Herein, we introduce three types of NLO-active units into a family of phosphate materials—a cation exhibiting a stereoactive lone pair, Pb^{2+}, a SOJT-distorted d^0 cation, W^{6+}, and a d^{10} cation, Zn^{2+}. The reported materials have the general chemical formula $A_3B_3CD_2O_{14}$ (A = Sr, Ba, or Pb; B = Mg or Zn; C = Te or W; D = P or V). Although the impact of NLO-active structural units in NLO materials has been studied before, it is uncommon to discover a family of NLO materials where the crystal chemistry and property effects derived from cation substitution can be comprehensively explored and understood.

We report the synthesis of six SHG-active materials in the Dugganite family: Sr$_3$Zn$_3$TeP$_2$O$_{14}$ (SZTP), Ba$_3$Zn$_3$TeP$_2$O$_{14}$ (BZTP), Pb$_3$Mg$_3$TeP$_2$O$_{14}$ (PMTP), Pb$_3$Zn$_3$TeP$_2$O$_{14}$ (PZTP), Pb$_3$Zn$_3$WP$_2$O$_{14}$ (PZWP), and Pb$_3$Zn$_3$TeV$_2$O$_{14}$ (PZTV). A communication regarding Pb$_3$Mg$_3$TeP$_2$O$_{14}$ has recently appeared;[13] this is the first time the other five have been reported.

Table 1. Crystal Data and Structure Refinement for $A_3B_3CD_2O_{14}$ (A = Sr, Ba, or Pb; B = Mg or Zn; C = Te or W; D = P or V)

formula	$Sr_3Zn_3TeP_2O_{14}$	$Ba_3Zn_3TeP_2O_{14}$	$Pb_3Zn_3TeP_2O_{14}$	$Pb_3Mg_3TeP_2O_{14}$	$Pb_3Zn_3TeV_2O_{14}$	$Pb_3Zn_3WP_2O_{14}$
T (K)	293(2)					
λ (Å)	0.71073					
fw	872.51	1021.67	1231.22	1108.04	1271.16	1287.47
crystal system	trigonal	trigonal	trigonal	trigonal	trigonal	trigonal
space group	$P321$	$P321$	$P321$	$P321$	$P321$	$P321$
a (Å)	8.2767(3)	8.4744(3)	8.3831(3)	8.4072(4)	8.608(2)	8.4151(3)
c (Å)	5.1763(4)	5.2818(4)	5.1930(4)	5.2158(5)	5.186(3)	5.1700(4)
Z	1	1	1	1	1	1
V (Å^3)	307.09(3)	328.50(3)	316.05(3)	319.27(4)	332.8(2)	317.06(3)
ρ (g/cm^3)	4.718	5.165	6.469	5.763	6.343	6.743
μ (mm^{-1})	21.367	16.732	48.003	42.168	46.665	54.613
R_{int}	0.0316	0.0166	0.0399	0.0249	0.0331	0.0282
completeness	99.7%	99.7%	100.0%	100.0%	100.0%	100.0%
GOF (F^2)	1.096	1.174	1.095	0.958	1.212	1.197
final R indices $[I > 2\sigma(I)]^a$	$R_1 = 0.0208$, $wR_2 = 0.0447$	$R_1 = 0.0161$, $wR_2 = 0.0375$	$R_1 = 0.0206$, $wR_2 = 0.0531$	$R_1 = 0.0140$, $wR_2 = 0.0328$	$R_1 = 0.0277$, $wR_2 = 0.0643$	$R_1 = 0.0170$, $wR_2 = 0.0402$
R indices (all data)	$R_1 = 0.0217$, $wR_2 = 0.0453$	$R_1 = 0.0161$, $wR_2 = 0.0375$	$R_1 = 0.0208$, $wR_2 = 0.0533$	$R_1 = 0.0144$, $wR_2 = 0.0330$	$R_1 = 0.0280$, $wR_2 = 0.0644$	$R_1 = 0.0170$, $wR_2 = 0.0402$
Flack factor	0.052(14)	0.05(4)	0.051(13)	0.031(9)	0.011(17)	0.371(15)
extinction coefficient	0.0071(12)	0.0064(7)	0.0150(11)	0.0098(6)	0.0157(11)	0.0140(7)
largest diff. peak and hole (e·Å^{-3})	0.820 and −0.734	1.744 and −0.794	1.590 and −1.294	0.920 and −0.623	2.120 and −1.585	1.507 and −1.064

$^a R_1 = \sum \lvert\lvert F_o\rvert - \lvert F_c\rvert\rvert / \sum \lvert F_o \rvert$ and $wR_2 = \left[\sum w (F_o^2 - F_c^2)^2 / \sum w F_o^4\right]^{1/2}$ for $F_o^2 > 2\sigma(F_o^2)$.

All of the reported compounds exhibit strong SHG responses and have potential applications as NLO materials ranging from the UV to the near-IR (200−5000 nm). The materials are isostructural and strongly SHG-active at 1064 nm. Through experimental chemical substitution, we are able to characterize the SHG response in materials with a stereoactive lone pair cation (Pb^{2+}) and without (Sr^{2+} and Ba^{2+}), as well as those containing SOJT-active (W^{6+}) or inactive (Te^{6+}) cations. By combining these results with density functional theory (DFT) calculations, we are able to disentangle the contribution of the NLO-active structural units to the SHG-active material family. We find that the largest increase in the SHG response occurs upon substitution of Pb^{2+} cations, due to the appearance of Pb 6s and 5p states at the band edges in the density of states. Furthermore, these results show that the presence of Te 5s states is also key to the enhancement of the NLO properties. Finally, through an analysis of the symmetry-breaking atomic displacements (SAMDs), we correlate the magnitude of the SHG response to several structural descriptors, such as rotations of the DO_4 (D = P^{5+} or V^{5+}) units, that may serve as a useful crystal chemistry feature for future materials design and discovery.

■ EXPERIMENTAL SECTION

Reagents. $SrCO_3$ (Aldrich Chemical Company. Inc., 98%), $BaCO_3$ (Fisher Scientific Company, 99%), PbO (Sigma-Aldrich, 99.9%), MgO (Alfa Aesar, 99%), ZnO (Alfa Aesar, 98%), $H_2TeO_4\cdot 2H_2O$ (Alfa Aesar, 99%), WO_3 (Alfa Aesar, 99.8%), $NH_4H_2PO_4$ (Alfa Aesar, 98%), and V_2O_5 (Sigma-Aldrich, 99.9%) were used as received.

Compound Synthesis. Polycrystalline samples of the title compounds were synthesized by conventional solid-state methods. Stoichiometric amounts of the reactants were ground thoroughly, packed tightly in a platinum crucible, and heated to 400 °C. The reaction was held at this temperature for 20 h to decompose carbonates, $NH_4H_2PO_4$, and $H_2TeO_4\cdot 2H_2O$. The temperature was increased to 950, 850, and 700 °C for $Ba_3Zn_3TeP_2O_{14}$ and $Sr_3Zn_3TeP_2O_{14}$, $Pb_3Mg_3TeP_2O_{14}$ and $Pb_3Zn_3TeP_2O_{14}$, and $Pb_3Zn_3WP_2O_{14}$ and $Pb_3Zn_3TeV_2O_{14}$, respectively, and held at these temperatures for 5 days with several intermittent grindings. The purity of the polycrystal-

line samples was confirmed by powder X-ray diffraction (XRD) measurements (see Figure S1 in the Supporting Information).

Powder X-ray Diffraction. The powder XRD measurements were carried out at room temperature on a PANalytical X'Pert PRO diffractometer equipped with Cu Kα radiation ($\lambda = 1.5418$ Å). Data were collected in the angular range of $2\theta = 10-70°$ with a scan step width of 0.008° and a scan time of 0.5 s.

Crystal Growth. Single crystals of the title compounds were grown from a high-temperature solution using TeO_2 or $Pb_3(PO_4)_2$ as the flux. For $Ba_3Zn_3TeP_2O_{14}$, $Sr_3Zn_3TeP_2O_{14}$, and $Pb_3Mg_3TeP_2O_{14}$, the polycrystalline samples were mixed thoroughly with TeO_2 at a molar ratio of the polycrystalline samples/TeO_2 = 1:3. The mixtures were heated in a platinum crucible to 950 °C and held at this temperature for 10 h. The temperature was reduced to 700 °C at a rate of 2 °C h^{-1} and cooled to room temperature at a rate of 10 °C h^{-1}. For $Pb_3Zn_3TeP_2O_{14}$ and $Pb_3Zn_3TeV_2O_{14}$, the polycrystalline samples were mixed thoroughly with TeO_2 at a molar ratio of the polycrystalline samples/TeO_2 = 1:2. The mixtures were heated in a platinum crucible to 800 °C and held at this temperature for 10 h. The temperature was reduced to 650 °C at a rate of 2 °C h^{-1} and cooled to room temperature at a rate of 10 °C h^{-1}. For $Pb_3Zn_3WP_2O_{14}$, the compound was mixed with $Pb_3(PO_4)_2$ at a molar ratio of PZWP/$Pb_3(PO_4)_2$ = 1:1. The mixtures were heated to 900 °C in a platinum crucible and kept this temperature for 10 h. The temperature was decreased to 700 °C at a rate of 2 °C h^{-1} and cooled to room temperature at a rate of 20 °C h^{-1}. The sub-millimeter-sized crystals grew as regular hexagonal-shaped prisms (Figure S2).

Single-Crystal X-ray Diffraction. The crystal structures of the reported materials were determined by single-crystal X-ray diffraction. Data were collected on a Bruker DUO platform diffractometer equipped with a 4K CCD area detector using graphite-monochromated Mo Kα radiation ($\lambda = 0.71073$ Å) and were integrated with the SAINT program.[14] A multiscan technique was applied for the absorption corrections. All structures were solved by direct methods using SHELXS-97.[15] All atoms in these structures were refined using full matrix least-squares techniques, and final least-squares refinement was on F_o^2 with data having $F_o^2 \geq 2\sigma(F_o^2)$. All structures were checked with PLATON.[16] Crystal data and structure refinement information for the title compounds are listed in Table 1, and their final refined atomic positions and isotropic thermal parameters, selected bond lengths, and angles are listed in Tables S1 and S2 in the Supporting Information.

Infrared Spectroscopy. The Fourier transform infrared spectroscopy (FTIR) spectra in the 400−4000 cm^{-1} range were recorded on a
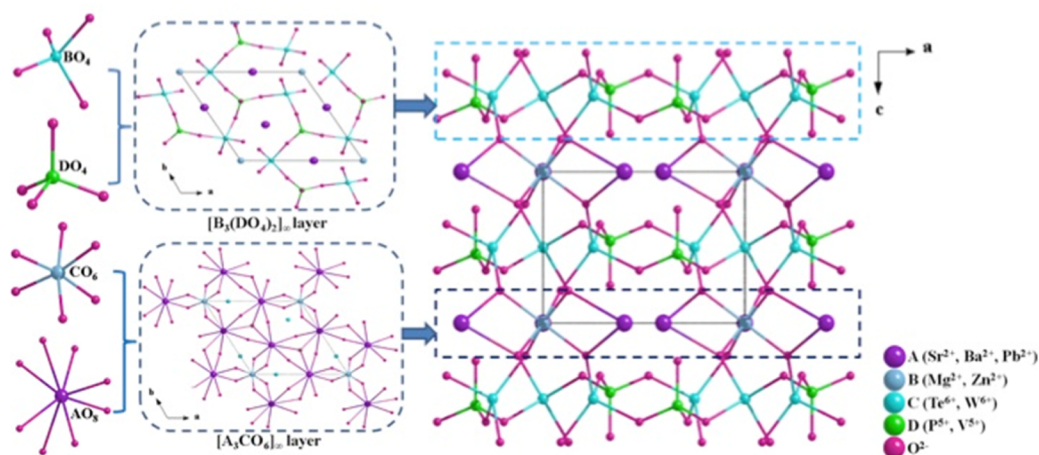
Figure 1. Ball-and-stick representation of $A_3B_3CD_2O_{14}$ (A = Sr, Ba, or Pb; B = Mg or Zn; C = Te or W; D = P or V).

Bruker Tensor 37 FTIR. The samples were mixed thoroughly with dried KBr. The IR data are shown in Figure S3 in the Supporting Information.

UV−Vis−NIR Diffuse Reflectance Spectrum. The UV−vis−NIR diffuse reflectance spectra were measured at room temperature with a Cary 5000 UV−vis−NIR spectrophotometer in the 200−2500 nm wavelength range.

Thermal Analysis. The thermal properties were measured on EXSTAR TG/DTA 6300 under flowing nitrogen gas.

Second-Order NLO Measurements. Powder SHG was measured by using the Kurtz−Perry method with Q-switched Nd:YAG lasers at 1064 nm.[17] Polycrystalline samples and KDP were ground and sieved into distinct particle size ranges (<20, 20−45, 45−63, 63−75, 75−90, 90−125, >125 μm). Sieved KDP powder was used as a reference. The samples were placed in 1 mm thick fused silica tubes and irradiated by a Q-switched Nd:YAG solid-state laser. The intensity of the frequency-doubled radiation from the samples was measured using a photomultiplier tube.

Electronic Structure Calculations. The density of states (DOS) calculations were performed using density functional theory[18] as implemented in the Vienna Ab initio Simulation Package (VASP)[19] with projector-augmented wave (PAW) pseudopotentials[20] and the PBEsol functional.[21] Calculations on the NCS structures used the experimental lattice constants and atomic positions. The hypothetical $P\bar{3}m1$ high-symmetry structures were generated with help from the PSEUDO tool, part of the Bilbao crystallographic server;[22] the internal atomic positions were then relaxed at the experimental lattice constants of the observed NCS structures using a 650 eV plane wave cutoff and a 5 × 5 × 7 Monkhorst−Pack k-point mesh.[23] The density of states were computed using a 650 eV plane wave cutoff and an increased 7 × 7 × 9 k-point mesh. The mode decompositions were performed using the ISODISTORT tool of the ISOTROPY software suite.[24] The nonlinear optical properties were computed using density functional perturbation theory as implemented in ABINIT[25] with a 650 eV plane wave cutoff and a 5 × 5 × 7 k-point mesh. Norm-conserving pseudopotentials were generated using the Troullier−Martins scheme.[26]

RESULTS AND DISCUSSION

Crystal Structures. The reported compounds are isostructural (Table 1) and may be described using the general formula $A_3B_3CD_2O_{14}$ (A = Sr^{2+}, Ba^{2+}, or Pb^{2+}; B = Mg^{2+} or Zn^{2+}; C = Te^{6+} or W^{6+}; D = P^{5+} or V^{5+}). A ball-and-stick representation of the structure is shown in Figure 1. The structures exhibit a three-dimensional framework composed of AO_8 (A = Sr^{2+}, Ba^{2+}, or Pb^{2+}) polyhedra, BO_4 (B = Mg^{2+} or Zn^{2+}) and DO_4 (D = P^{5+} or V^{5+}) tetrahedra, and CO_6 (C = Te^{6+} or W^{6+}) octahedra. In the *ab*-plane, the BO_4 and DO_4 tetrahedra are corner-shared and form a two-dimensional $[B_3(DO_4)_2]_\infty$ layer, and the AO_8 polyhedra and

CO_6 octahedra are edge-shared and form a two-dimensional $[A_3CO_6]_\infty$ layer. These layers alternate and connect along the *c*-axis by sharing oxygen atoms to create the three-dimensional framework.

With respect to metal−oxygen bonding, the A cations (Sr^{2+}, Ba^{2+}, or Pb^{2+}) are bonded to eight oxygen atoms with bond lengths ranging from 2.492(4) to 2.949(7) Å (A = Sr^{2+}), 2.619(4) to 2.977(4) Å (A = Ba^{2+}), and 2.341(4) to 3.081(13) Å (A = Pb^{2+}). In all the Pb-containing compounds, two short Pb−O bond lengths ranging from 2.341(4) to 2.379(7) Å and six longer Pb−O bond lengths ranging from 2.658(11) to 2.949(7) Å are observed. The variable Pb−O bond lengths suggest that the lone pair on the Pb^{2+} cations is stereochemically active (see Figure S4). The B (Mg^{2+} and Zn^{2+}) and D cations (P^{5+} and V^{5+}) are tetrahedrally coordinated to four oxygen atoms. The B cation bond lengths range from 1.939(4) to 1.957(4) Å (B = Mg^{2+}) and 1.905(4) to 2.039(4) Å (B = Zn^{2+}), whereas for the D cations, the distances are 1.518(12)−1.545(7) Å (D = P^{5+}) and 1.674(16)−1.733(10) Å (D = V^{5+}). Finally, octahedral coordination is observed for the C cations, Te^{6+} and W^{6+}. The Te−O bond lengths range from 1.912(6) to 1.926(9) Å, whereas one W−O bond distance of 1.911(6) Å is observed. Bond valence calculations[27] resulted in bond valence sums of 1.86 (Sr^{2+}), 2.12 (Ba^{2+}), 1.82−1.94 (Pb^{2+}), 2.01 (Mg^2), 1.97−2.12 (Zn^{2+}), 5.86−6.08 (Te^{6+}), 6.16 (W^{6+}), 4.75−4.98 (P^{5+}), and 5.05 (V^{5+}). Oxygen valences range from 1.66 to 2.09.

Infrared Measurements. The IR spectrum is shown in Figure S3. It is clear that $Sr_3Zn_3TeP_2O_{14}$, $Ba_3Zn_3TeP_2O_{14}$, $Pb_3Zn_3TeP_2O_{14}$, and $Pb_3Mg_3TeP_2O_{14}$ exhibit similar IR spectra. The symmetric and asymmetric PO_4 vibrations are observed at 940−980 cm^{-1} and 1000−1150 cm^{-1}, respectively. For $Pb_3Zn_3WP_2O_{14}$ and $Pb_3Zn_3TeV_2O_{14}$, the band around 806 cm^{-1} is attributed to the stretching of the W−O bond of the WO_6 octahedra, and the bands in the range from 773 to 892 cm^{-1} can be attributed to the stretching of the V−O bond of the VO_4 tetrahedra. The bands in the range from 738 to 400 cm^{-1} mainly result from the Pb−O, Te−O, Zn−O, and Mg−O bonds. These assignments are consistent with those previously reported.[28]

Thermal Behavior. The TG/DTA curves of these compounds are shown in Figure S5 in the Supporting Information. It is clear that all of the materials melt incongruently. $Sr_3Zn_3TeP_2O_{14}$, $Ba_3Zn_3TeP_2O_{14}$, $Pb_3Mg_3TeP_2O_{14}$, and $Pb_3Zn_3TeP_2O_{14}$ are stable up to 1000 °C. The weight loss around 1050 °C is caused by the

decomposition of the compounds, which is confirmed by the powder XRD on the residues after TG/DTA measurement. The residues of $Sr_3Zn_3TeP_2O_{14}$ and $Ba_3Zn_3TeP_2O_{14}$ are a mixture of ZnO, $Sr_3(PO_4)_2/Sr_3(PO_4)_2$, and $Sr_3Zn_3TeP_2O_{14}/Ba_3Zn_3TeP_2O_{14}$ (Figures S6a,b). The residues for $Pb_3Zn_3TeP_2O_{14}$ are ZnO, $Pb_3(PO_4)_2$, and other unknown phases (Figure S6c). The residues for $Pb_3Mg_3TeP_2O_{14}$ are $Pb_3(PO_4)_2$, $Mg_3(PO_4)_2$, and other unknown phases (Figure S6d). For $Pb_3Zn_3WP_2O_{14}$ and $Pb_3Zn_3TeV_2O_{14}$, there is no obvious weight loss in their TG curves, but there is more than one endothermic/exothermic peak on the heating/cooling curves, and their residues after TG/DTA are shown by powder XRD measurements to be ZnO and some unknown phases (Figure S6e,f).

UV−Vis Diffuse Reflectance Spectrum. The UV−vis diffuse reflectance spectra were also collected (see Table 2).

Table 2. SHG Responses, Absorption Edges, Experimental Band Gaps, and Calculated SHG Coefficients for the $A_3B_3CD_2O_{14}$ (A = Sr, Ba, or Pb; B = Mg or Zn; C = Te or W; D = P or V) Compounds

compound	PSHG at 1064 nm (×KDP)	absorption edge (nm)	band gap (eV)	DFT SHG (d_{11} pm/V)
$Sr_3Zn_3TeP_2O_{14}$	2.8	222	5.58	2.27
$Ba_3Zn_3TeP_2O_{14}$	3	218	5.69	2.33
$Pb_3Zn_3WP_2O_{14}$	7	317	3.91	4.62
$Pb_3Zn_3TeV_2O_{14}$	12.5	337	3.68	6.95
$Pb_3Mg_3TeP_2O_{14}$	13.5	250	4.96	5.98
$Pb_3Zn_3TeP_2O_{14}$	13.5	253	4.90	5.19

$Ba_3Zn_3TeP_2O_{14}$, $Sr_3Zn_3TeP_2O_{14}$, $Pb_3Mg_3TeP_2O_{14}$, and $Pb_3Zn_3TeP_2O_{14}$ exhibit absorption edges below 300 nm, which suggests that these materials have potential NLO applications in the UV region. Comparing the absorption edges of these four compounds, we observe that $Ba_3Zn_3TeP_2O_{14}$ and $Sr_3Zn_3TeP_2O_{14}$ have the shortest absorption edge, ∼220 nm, whereas $Pb_3Mg_3TeP_2O_{14}$ and $Pb_3Zn_3TeP_2O_{14}$ have slightly red-shifted absorption edges (i.e., 250 and 253 nm, respectively), attributable to the Pb^{2+} atoms replacing the alkaline earth metals. The absorption edges of $Pb_3Zn_3WP_2O_{14}$ and $Pb_3Zn_3TeV_2O_{14}$ are further red-shifted to 317 and 337 nm due to the W^{6+} and V^{5+} cations.

Second Harmonic Generating Properties and Structure−Property Relationships. The reported materials crystallize in the noncentrosymmetric chiral space group $P321$. Powder SHG measurements using 1064 nm radiation revealed efficiencies ranging from 3 × KDP to 13.5 × KDP (see Table 2). Additional particle size versus SHG efficiency measurements indicate that all the materials are type I phase-matchable (see Figure 2). Comparing the SHG efficiencies, we observe that the Pb^{2+}-containing compounds have larger SHG responses. This suggests that the stereoactive lone pair on Pb^{2+} has a positive impact on the SHG efficiency.

We also investigated this series of NLO materials using first-principles density functional theory calculations. First, we computed the SHG coefficients for each of the six compounds. For point group 32, there are three equivalent nonzero components of the SHG tensor (after consideration of Kleinmann symmetry): $d_{11} = -d_{12} = -d_{26}$.[29] In general, the experimental trend is well captured by our calculated SHG coefficients (Table 2), and although we find that the SHG coefficients of $Pb_3Mg_3TeP_2O_{14}$ and $Pb_3Zn_3TeP_2O_{14}$ are large
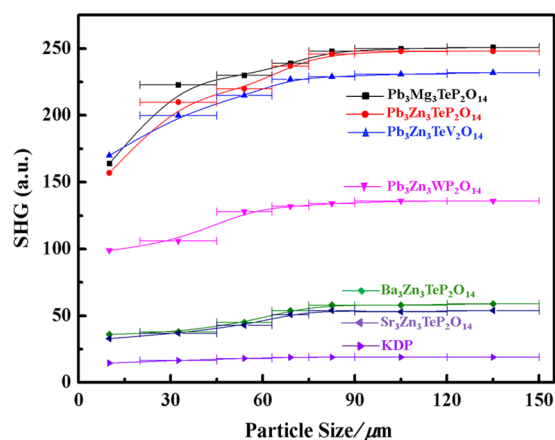
Figure 2. Phase-matching curves for KDP, $Sr_3Zn_3TeP_2O_{14}$, $Ba_3Zn_3TeP_2O_{14}$, $Pb_3Zn_3WP_2O_{14}$, $Pb_3Zn_3TeV_2O_{14}$, $Pb_3Zn_3TeP_2O_{14}$, and $Pb_3Mg_3TeP_2O_{14}$. The solid curves are drawn to guide the eye and are not a fit to the data.

among the family, as observed in the experimental data, the absolute values are approximately half as large as that in the experiment. Furthermore, we found $Pb_3Zn_3TeV_2O_{14}$ to exhibit the largest response when experimentally $Pb_3Mg_3TeP_2O_{14}$ and $Pb_3Zn_3TeP_2O_{14}$ are both higher.

To better understand the experimental trend in terms of the electronic structure of these materials, we computed the atom-resolved DOS for each member of this series (Figure 3, plotted in
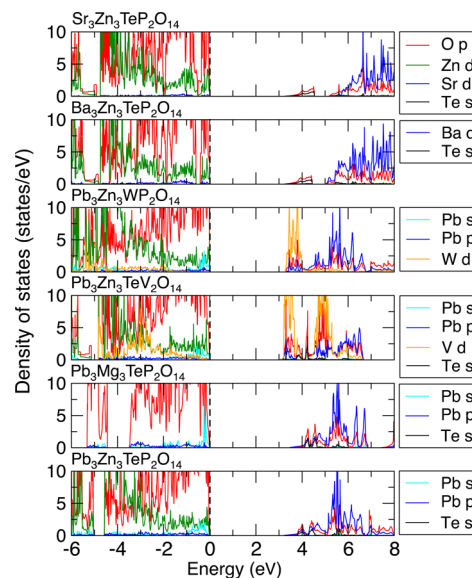

Figure 3. Atom-resolved density of states for each of the synthesized NLO materials. In each case, the O 2p states and Zn 3d states are colored red and green, respectively, while the other colors represent other states derived from the chemistry examined. The Fermi level is set to 0 eV (broken black line).

order from lowest to highest experimental SHG response). First, we find that the Pb-free compounds, $Sr_3Zn_3TeP_2O_{14}$ and $Ba_3Zn_3TeP_2O_{14}$, exhibit a very similar density of states, with O 2p and Zn 3d states forming the top of the valence band (features characteristic of all Zn-containing materials in this series) and O 2p and Te 5s states forming the bottom of the conduction band. The Sr and Ba d states are high in energy, so their substitution

does not alter these band edges, and therefore, they have a negligible effect on the NLO properties.

Substitution of Pb, however, introduces Pb 6s states at the top of the valence band and Pb 6p states at the bottom of the conduction band (a well-known feature of Pb-containing materials)[5a,13,30] and greatly enhances the SHG response through lone-pair activity (Figure S4). In $Pb_3Zn_3WP_2O_{14}$ and $Pb_3Zn_3TeV_2O_{14}$, the substitution of W^{6+} and V^{5+} results in d states at the bottom of the conduction band, reducing the gap, and due to the change in parity of the dominant orbitals leads to a reduction in the SHG response relative to $Pb_3Mg_3TeP_2O_{14}$ and $Pb_3Zn_3TeP_2O_{14}$. Furthermore, $Pb_3Zn_3WP_2O_{14}$ exhibits the lowest response of the Pb-containing compounds, which allows us to deduce that the presence of the Te 5s states in the former compounds enhances the SHG response. $Pb_3Mg_3TeP_2O_{14}$ and $Pb_3Zn_3TeP_2O_{14}$ have a similar DOS, resulting in a similar SHG intensity.

To further elucidate the structure−NLO property relationship, we characterized the inversion lifting atomic displacements using a symmetry-adapted mode decomposition[31] following the approach of Wu et al., who applied this method to characterize the cooperative inversion symmetry lifting displacements in nonlinear optical materials.[5b] For each compound, we generated a hypothetical high-symmetry structure in the centrosymmetric space group $P\bar{3}m1$ (Figure 4a) and found that two displacive
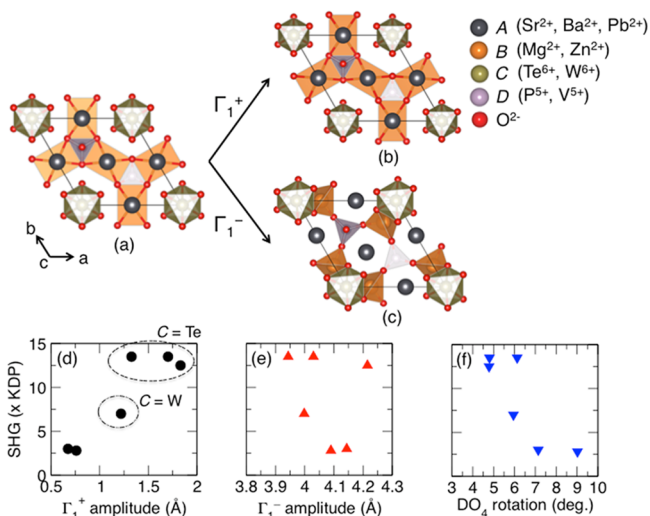
Figure 4. (a) High-symmetry $P\bar{3}m1$ phase with the atomic displacements making up the (b) Γ_1^+ mode or (c) Γ_1^- mode. The SHG response as a function of the amplitude of the (d) Γ_1^+ mode, (e) Γ_1^- mode, and (f) DO_4 rotations.

modes relate this centrosymmetric structure to the observed $P321$ chiral structure. The first mode is fully symmetric, given by the irreducible representation (irrep) Γ_1^+, and does not result in any change in symmetry; the mode consists of small oxygen displacements that contract the TeO_6 or WO_6 octahedra (Figure 4b). The second mode, characterized by irrep Γ_1^-, lifts inversion symmetry in the structure and allows for SHG. The chiral mode consists of an off-centering of the A- and B-site atoms (A = Sr, Ba, or Pb; B = Mg or Zn) and cooperative oxygen displacements that act to form the corner-shared BO_4−CO_6−DO_4 network (Figure 4c). Interestingly, the magnitude of the Γ_1^+ mode is strongly correlated ($R^2 = 0.82$) with the magnitude of the SHG response in this series of compounds (Figure 4d), whereas Γ_1^- is poorly and possibly anticorrelated (Figure 4e). Because Γ_1^+ results in

greater Te−O or W−O overlap, that is, by shortening the Te−O or W−O bonds, we deduce that the Te 5s states are an important electronic feature leading to the enhanced SHG response in this family, consistent with our DOS analysis. Indeed, the Pb-based compounds containing Te exhibit a higher Γ_1^+ mode amplitude and SHG response than the phase containing W, that is, SHG ($Pb_3Zn_3TeP_2O_{14}$, $Pb_3Zn_3TeV_2O_{14}$) > SHG ($Pb_3Zn_3WP_2O_{14}$).

Energetically, the amplitude of Γ_1^+ in $P321$ becomes nonzero only in the presence of the soft Γ_1^- mode; that is, the atomic displacements described by Γ_1^+ raise the energy of the system if they are frozen into the high-symmetry structure. Because Γ_1^- may be used as the primary order parameter to capture the hypothetical symmetry breaking, there should be some component of it that correlates with the observed variations in the SHG responses among the compounds. We therefore decomposed the total Γ_1^- mode into contributions from each atom and found that displacements of the oxygen atoms comprising the DO_4 (D = P or V) tetrahedra, which correspond directly to the magnitude of the rotation of these units, are able to describe the trend in the NLO properties (Figure 4f). Those compounds with *large rotations* ($Sr_3Zn_3TeP_2O_{14}$ and $Ba_3Zn_3TeP_2O_{14}$) exhibit a small SHG response, whereas those with the *smallest rotations* ($Pb_3Zn_3TeP_2O_{14}$ and $Pb_3Mg_3TeP_2O_{14}$) exhibit the largest SHG response.

■ CONCLUSION

We designed and synthesized a family of NLO-active chiral phosphate materials with large SHG responses and absorption edges that can be utilized for NLO applications ranging from the UV to the near-IR. Through chemical substitution, we were able to systematically discern the effects of acentric structural units on the NLO properties. Using first-principles electronic structure calculations, we investigated the result of this substitution on the character of the band edges across the family and showed that the presence of Pb^{2+} and Te^{6+} cations are crucial to maximizing the SHG response. Finally, an analysis of the inversion lifting atomic displacements revealed the crystal chemistry contributions to the NLO properties, further demonstrating the importance of the Te 5s states. We anticipate that our approach applied here to understand the electronic and atomic structural contributions may be particularly useful for designing and optimizing optical responses in other multicomponent complex mineral families.

■ ASSOCIATED CONTENT

⑤ Supporting Information

The Supporting Information is available free of charge on the ACS Publications website at DOI: 10.1021/jacs.6b02203.

> X-ray data for BZTP (CIF)
> Experimental and calculated XRD patterns; crystal photo and theoretical morphology of $Pb_3Mg_3TeP_2O_{14}$; IR spectrum; computed electron localization function; DTA/TG curves; X-ray diffraction pattern of the residue in the platinum pan after DTA/TG measurement; atomic coordinates, equivalent isotropic displacement parameters, and the bond valence sums of each atom; selected bond distances and angles (PDF)

■ AUTHOR INFORMATION

Corresponding Authors

*jrondinelli@northwestern.edu

*psh@uh.edu

Notes

■ ACKNOWLEDGMENTS

■ REFERENCES

(1) (a) Monroe, C. *Nature* **2002**, *416*, 238. (b) William, M. S.; Jyotirmoy, M. *Laser Material Processing*; Springer: New York, 2010. (c) Jiang, X.; Kang, L.; Luo, S.; Gong, P.; Lee, M.-H.; Lin, Z. *Int. J. Mod. Phys. B* **2014**, *28*, 1430018.

(2) (a) Becker, P. *Adv. Mater.* **1998**, *10*, 979. (b) Keszler, D. A. *Curr. Opin. Solid State Mater. Sci.* **1996**, *1*, 204. (c) Halasyamani, P. S.; Poeppelmeier, K. R. *Chem. Mater.* **1998**, *10*, 2753.

(3) (a) Chen, C. T.; Wu, B. C.; Jiang, A. D.; You, G. M. *Sci. Sin. B* **1985**, *15*, 235. (b) Chen, C. T.; Wu, Y. C.; Jiang, A. D.; Wu, B. C.; You, G. M.; Li, R. K.; Lin, S. J. *J. Opt. Soc. Am. B* **1989**, *6*, 616. (c) Nishioka, M.; Kanoh, A.; Yoshimura, M.; Mori, Y.; Sasaki, T. *J. Cryst. Growth* **2005**, *279*, 76. (d) Chen, C. T.; Wang, G. L.; Wang, X. Y.; Xu, Z. Y. *Appl. Phys. B: Lasers Opt.* **2009**, *97*, 9. (e) Chen, C.; Wang, Y.; Wu, B.; Wu, K.; Zeng, W.; Yu, L. *Nature* **1995**, *373*, 322. (f) Dmitriev, V. G.; Gurzadyan, G. G.; Nikogosyan, D. N. *Handbook of Nonlinear Optical Crystals*; Springer: New York, 1999.

(4) (a) Huang, H.; Liu, L.; Jin, S.; Yao, W.; Zhang, Y.; Chen, C. *J. Am. Chem. Soc.* **2013**, *135*, 18319. (b) Wang, S.; Ye, N. *J. Am. Chem. Soc.* **2011**, *133*, 11458. (c) Wang, S. C.; Ye, N.; Li, W.; Zhao, D. *J. Am. Chem. Soc.* **2010**, *132*, 8779. (d) Huang, H.; Yao, J.; Lin, Z.; Wang, X.; He, R.; Yao, W.; Zhai, N.; Chen, C. *Angew. Chem., Int. Ed.* **2011**, *50*, 9141.

(5) (a) Dong, X.; Jing, Q.; Shi, Y.; Yang, Z.; Pan, S.; Poeppelmeier, K. R.; Young, J.; Rondinelli, J. M. *J. Am. Chem. Soc.* **2015**, *137*, 9417. (b) Wu, H.; Yu, H.; Yang, Z.; Hou, X.; Su, X.; Pan, S.; Poeppelmeier, K. R.; Rondinelli, J. M. *J. Am. Chem. Soc.* **2013**, *135*, 4215. (c) Wu, H.; Pan, S.; Poeppelmeier, K. R.; Li, H.; Jia, D.; Chen, Z.; Fan, X.; Yang, Y.; Rondinelli, J. M.; Luo, H. *J. Am. Chem. Soc.* **2011**, *133*, 7786. (d) Wang, X.; Zhang, G.; Zhao, Y.; Fan, F.; Liu, H.; Fu, P. *Opt. Mater.* **2007**, *29*, 1658. (e) Zhang, M.; Su, X.; Pan, S.; Wang, Z.; Zhang, H.; Yang, Z.; Zhang, B.; Dong, L.; Wang, Y.; Zhang, F.; Yang, Y. *J. Phys. Chem. C* **2014**, *118*, 11849. (f) Yu, H.; Wu, H.; Pan, S.; Yang, Z.; Su, X.; Zhang, F. *J. Mater. Chem.* **2012**, *22*, 9665.

(6) (a) Yu, H.; Wu, H.; Pan, S.; Yang, Z.; Hou, X.; Su, X.; Jing, Q.; Poeppelmeier, K. R.; Rondinelli, J. M. *J. Am. Chem. Soc.* **2014**, *136*, 1264. (b) Wu, H.; Yu, H.; Pan, S.; Huang, Z.; Yang, Z.; Su, X.; Poeppelmeier, K. R. *Angew. Chem., Int. Ed.* **2013**, *52*, 3406. (c) Zhao, S. G.; Gong, P. F.; Bai, L.; Xu, X.; Zhang, S. Q.; Sun, Z. H.; Lin, Z. S.; Hong, M. C.; Chen, C. T.; Luo, J. H. *Nat. Commun.* **2014**, *5*, 4019.

(7) (a) Zhao, S.; Gong, P.; Luo, S.; Bai, L.; Lin, Z.; Tang, Y.; Zhou, Y.; Hong, M.; Luo, J. *Angew. Chem.* **2015**, *127*, 4291. (b) Zhao, S.; Gong, P.; Luo, S.; Bai, L.; Lin, Z.; Ji, C.; Chen, T.; Hong, M.; Luo, J. *J. Am. Chem. Soc.* **2014**, *136*, 8560. (c) Yu, P.; Wu, L.-M.; Zhou, L.-J.; Chen, L. *J. Am. Chem. Soc.* **2014**, *136*, 480. (d) Sun, T.; Shan, P.; Chen, H.; Liu, X.; Liu, H.; Chen, S.; Cao, Y. a.; Kong, Y.; Xu, J. *CrystEngComm* **2014**, *16*, 10497.

(8) Yu, H.; Zhang, W.; Young, J.; Rondinelli, J. M.; Halasyamani, P. S. *Adv. Mater.* **2015**, *27*, 7380.

(9) (a) Zhang, H.; Zhang, M.; Pan, S.; Dong, X.; Yang, Z.; Hou, X.; Wang, Z.; Chang, K. B.; Poeppelmeier, K. R. *J. Am. Chem. Soc.* **2015**, *137*, 8360. (b) Zhang, G.; Li, Y.; Jiang, K.; Zeng, H.; Liu, T.; Chen, X.; Qin, J.; Lin, Z.; Fu, P.; Wu, Y.; Chen, C. *J. Am. Chem. Soc.* **2012**, *134*, 14818.

(10) (a) Song, J. L.; Hu, C. L.; Xu, X.; Kong, F.; Mao, J. G. *Angew. Chem., Int. Ed.* **2015**, *54*, 3679. (b) Sun, C. F.; Hu, C. L.; Xu, X.; Yang, B. P.; Mao, J. G. *J. Am. Chem. Soc.* **2011**, *133*, 5561. (c) Sun, C. F.; Hu, C. L.; Xu, X.; Ling, J. B.; Hu, T.; Kong, F.; Long, X. F.; Mao, J. G. *J. Am. Chem. Soc.* **2009**, *131*, 9486.

(11) (a) Nguyen, S. D.; Yeon, J.; Kim, S.-H.; Halasyamani, P. S. *J. Am. Chem. Soc.* **2011**, *133*, 12422. (b) Kim, S. H.; Yeon, J.; Halasyamani, P. S. *Chem. Mater.* **2009**, *21*, 5335. (c) Chang, H. Y.; Kim, S. H.; Ok, K. M.; Halasyamani, P. S. *J. Am. Chem. Soc.* **2009**, *131*, 6865. (d) Chang, H. Y.; Kim, S. H.; Halasyamani, P. S.; Ok, K. M. *J. Am. Chem. Soc.* **2009**, *131*, 2426.

(12) (a) Zhang, W. L.; Cheng, W. D.; Zhang, H.; Geng, L.; Lin, C. S.; He, Z. Z. *J. Am. Chem. Soc.* **2010**, *132*, 1508. (b) Inaguma, Y.; Yoshida, M.; Katsumata, T. *J. Am. Chem. Soc.* **2008**, *130*, 6704.

(13) Yu, H.; Zhang, W.; Young, J.; Rondinelli, J. M.; Halasyamani, P. S. *J. Am. Chem. Soc.* **2016**, *138*, 88.

(14) *SAINT*, version 7.60A; Bruker Analytical X-ray Instruments, Inc.: Madison, WI, 2008.

(15) Sheldrick, G. M. *SHELXTL*, version 6.14; Bruker Analytical X-ray Instruments, Inc.: Madison, WI, 2003.

(16) Spek, A. L. *J. Appl. Crystallogr.* **2003**, *36*, 7.

(17) (a) Kurtz, S. K.; Perry, T. T. *J. Appl. Phys.* **1968**, *39*, 3798. (b) Ok, K. M.; Chi, E. O.; Halasyamani, P. S. *Chem. Soc. Rev.* **2006**, *35*, 710.

(18) Hohenberg, P.; Kohn, W. *Phys. Rev.* **1964**, *136*, B864.

(19) (a) Kresse, G.; Hafner, J. *Phys. Rev. B: Condens. Matter Mater. Phys.* **1993**, *47*, 558. (b) Kresse, G.; Furthmuller. *Comput. Mater. Sci.* **1996**, *6*, 15.

(20) Blöchl, P. E. *Phys. Rev. B: Condens. Matter Mater. Phys.* **1994**, *50*, 17953.

(21) Perdew, J. P.; Ruzsinszky, A.; Csonka, G. I.; Vydrov, O. A.; Scuseria, G. E.; Constantin, L. A.; Zhou, X.; Burke, K. *Phys. Rev. Lett.* **2008**, *100*, 136406.

(22) Kroumova, E.; Aroyo, M. I.; Perez-Mato, J. M.; Ivantchev, S.; Igartua, J. M.; Wondratschek, H. *J. Appl. Crystallogr.* **2001**, *34*, 783.

(23) Monkhorst, H. J.; Pack, J. D. *Phys. Rev. B* **1976**, *13*, 5188.

(24) Campbell, B. J.; Stokes, H. T.; Tanner, D. E.; Hatch, D. M. *J. Appl. Crystallogr.* **2006**, *39*, 607.

(25) Gonze, X.; Amadon, B.; Anglade, P. M.; Beuken, J. M.; Bottin, F.; Boulanger, P.; Bruneval, F.; Caliste, D.; Caracas, R.; Côté, M.; Deutsch, T.; Genovese, L.; Ghosez, P.; Giantomassi, M.; Goedecker, S.; Hamann, D. R.; Hermet, P.; Jollet, F.; Jomard, G.; Leroux, S.; Mancini, M.; Mazevet, S.; Oliveira, M. J. T.; Onida, G.; Pouillon, Y.; Rangel, T.; Rignanese, G. M.; Sangalli, D.; Shaltaf, R.; Torrent, M.; Verstraete, M. J.; Zerah, G.; Zwanziger, J. W. *Comput. Phys. Commun.* **2009**, *180*, 2582.

(26) Troullier, N.; Martins, J. L. *Phys. Rev. B: Condens. Matter Mater. Phys.* **1991**, *43*, 1993.

(27) Brown, I. D.; Altermatt, D. *Acta Crystallogr., Sect. B: Struct. Sci.* **1985**, *41*, 244.

(28) (a) Wang, Y.; Pan, S.; Su, X.; Yang, Z.; Dong, L.; Zhang, M. *Inorg. Chem.* **2013**, *52*, 1488. (b) Kang, J.; Yang, Y.; Pan, S.; Yu, H.; Zhou, Z. *J. Mol. Struct.* **2014**, *1056*, 79. (c) Yeon, J.; Kim, S.-H.; Nguyen, S. D.; Lee, H.; Halasyamani, P. S. *Inorg. Chem.* **2012**, *51*, 2662.

(29) (a) Kleinman, D. A. *Phys. Rev.* **1962**, *126*, 1977. (b) Powell, R. C. *Symmetry, Group Theory, and the Physical Properties of Crystals*; Springer: New York, 2010.

(30) (a) Stoltzfus, M. W.; Woodward, P. M.; Seshadri, R.; Klepeis, J.-H.; Bursten, B. *Inorg. Chem.* **2007**, *46*, 3839. (b) Walsh, A.; Payne, D. J.; Egdell, R. G.; Watson, G. W. *Chem. Soc. Rev.* **2011**, *40*, 4455.

(31) Perez-Mato, J. M.; Orobengoa, D.; Aroyo, M. I. *Acta Crystallogr., Sect. A: Found. Crystallogr.* **2010**, *66*, 558.